Comparison of $MnCo_2O_4$ coated Crofer 22 H, 441, 430 as interconnects for intermediate-temperature solid oxide fuel cell stacks

Talic, Belma; Venkatachalam, Vinothini; Hendriksen, Peter Vang; Kiebach, Ragnar

Published in:
Journal of Alloys and Compounds

Link to article, DOI:
10.1016/j.jallcom.2019.153229

Publication date:
2020

Document Version
Peer reviewed version

Comparison of $MnCo_2O_4$ coated Crofer 22 H, 441, 430 as interconnects for intermediate-temperature solid oxide fuel cell stacks

Belma Talic[a,*] Vinothini Venkatachalam[a,1], Peter Vang Hendriksen[a], Ragnar Kiebach[a]

[a] *Department of Energy Conversion and Storage, Technical University of Denmark, Frederiksborgvej 399, DK-4000 Roskilde, Denmark*

** Corresponding author. E-mail: betal@dtu.dk*

Abstract.

The low-cost ferritic steel grades 441 and 430 are benchmarked against the specialty grade Crofer 22 H as possible interconnect materials for intermediate temperature solid oxide fuel cells. The steels are either pre-oxidized or coated with $MnCo_2O_4$. The composition and growth rate of the oxide scales in air is evaluated over a period of 2000 h at 650, 700 and 750 °C. The $MnCo_2O_4$ coating is found to reduce the thickness of the oxide scale on all three steels at 700 and 750 °C. The greatest protective effect is achieved on Crofer 22 H. A SiO_2 scale is formed at the Cr_2O_3/steel interface after oxidation for all three steels, but it remains discontinuous during the evaluated period. The $MnCo_2O_4$ coating provides sufficient protection to make the low-cost steels 441 and 430 promising interconnect materials for operation at 650-700 °C. For higher operation temperatures, 441 is not applicable due to poor scale adhesion.

Keywords: Solid oxide fuel cell; Interconnect, Ferritic stainless steel; High temperature corrosion; Coating

1 Introduction

Solid oxide fuel cells (SOFC) offer a clean and efficient way of converting H_2 and various hydrocarbons to electrical energy. To attain a usable voltage and power output, multiple SOFCs are typically stacked and connected in series via interconnects. Recently, much of the SOFC research and development has focused on decreasing the SOFC operating temperature from 750-850 °C to 600-700 °C, in part motivated by the wish to minimize thermally activated degradation processes and thereby increase the SOFC lifetime [1,2]. A lower operating temperature also allows the use of cheaper materials for the auxiliary components, such as the interconnect material, stack casing, and up- and down-stream heat exchangers.

Ferritic stainless steels (FSS) are attractive for the application as the SOFC interconnect material due to their low cost, ease of manufacturing, appropriate thermal expansion coefficient and good mechanical properties [3–5]. However, the use of FSS also presents some challenges. Thermal growth of the oxide scale, consisting mainly of semiconducting Cr_2O_3, leads to an increase in the electrical resistance with time [6]. For long operation times and thin components, growth of the oxide scale may deplete the Cr

[1] Present address: School of Metallurgy and Materials, University of Birmingham, B15 2SE, UK

content in the steel below the critical level where break-away oxidation occurs (typically 15-16 wt.% Cr) [7,8]. Furthermore, volatilization of Cr(VI) species from the scale surface has been shown to cause degradation of the electrical performance of the SOFC oxygen electrode [9–11].

To increase the lifetime of the FSS interconnect, several steels have been developed specifically for the application in SOFC stacks, for example Crofer 22 APU, Crofer 22 H, E-brite, Sanergy HT and ZMG232L. Some common features of these alloys are (i) a high Cr-content to ensure a sufficiently large "Cr-reservoir" for long term stability [12], (ii) minor additions of Mn (< 1 wt.%) to form an outer $(Mn,Cr)_3O_4$ scale that reduces, but not eliminates, Cr-volatilization [13], and (iii) addition of rare-earth elements such as La or Zr for improved oxidation resistance and scale adherence [14,15]. However, despite the advances made by tailoring the alloy chemistry, even these highly specialized alloys need to be coated to sufficiently suppress the Cr volatilization [13,16].

Among the different materials evaluated as protective coatings for SOFC interconnects, Co and Mn based spinel oxides are considered very promising, having been shown to both reduce Cr evaporation and the electrical resistance across the interconnect [17–21]. By coating Crofer 22 APU with e.g. $MnCo_2O_4$ the oxidation rate is sufficiently reduced to enable an acceptable interconnect lifetime (> 40 000 h at 800 °C) [17]. However, Crofer 22 APU and similar alloys specifically developed for interconnect application are expensive and typically only available from a single manufacturer, thus making the solution unattractive for commercial applications. In this perspective, commodity FSSs such as 441 and 430 would be a more attractive choice due to their lower cost and higher availability.

Previous studies have indicated the potential of using 441 and 430 steels as the interconnect material, but have also identified some challenges such as formation of insulating SiO_2 scales, poor scale adherence, and a lower oxidation resistance compared to the more specialized alloys [22–32]. The majority of these investigations have been carried out at elevated temperatures (750-850 °C) and there are only a few studies reporting on the performance of low-cost FSSs below 700 °C [33–35]. As oxidation is a thermally activated process, the reduction in the SOFC operating temperature may enable the use of the low-cost steels despite the previously identified challenges. However, protective coatings such as $MnCo_2O_4$ are still needed when the temperature is decreased, due to significant Cr volatilization even at 650 °C [36],

Here, we investigate the oxidation resistance of bare and $MnCo_2O_4$ coated FSS in the temperature range of 650-750 °C. Two low-cost commodity stainless steels, 441 and 430, are benchmarked against the more specialized Crofer 22 H grade.

2 Material and methods

Steel sheets of 0.3 mm thickness with the compositions given in Table 1 were used in this work. The sheets were cut into 2x2 cm^2 coupons and a 3 mm hole was punched in one of the corners for mounting purposes. The coupons were cleaned in acetone and then ethanol for 10 min each in an ultrasonic bath. A $MnCo_2O_4$ (MCO) coating was deposited on the coupons by electrophoretic deposition (EPD). For this purpose, a suspension was prepared by mixing 2 wt.% of $MnCo_2O_4$ powder (Fuel Cell Materials, 5.1 m^2/g surface area) with isopropanol (Alfa Aesar, 99.7%) and ethanol (Plum A/S, 99.9%) (50:50 by volume) and iodine (0.5 g L^{-1}, Sigma Aldrich, 99.8%). The suspension was ball milled for 48 h before use (500 mL

PE-bottle, Ø10 mm YSZ milling rods). The EPD set-up consisted of a 150 ml Teflon box with the steel coupons mounted in parallel between two stainless steel counter electrodes at 15 mm distance on each side. The deposition was carried out at 60 V for 60 s. Further details about the coating procedure may be found in [37].

After coating, the samples were left to dry at room temperature (1-2 h) and subsequently sintered at 900 °C in air for 2 h (120 °C h^{-1} heating and cooling rate). Non-coated (bare) steel coupons were pre-oxidized under the same conditions (900 °C, 2h, air) to serve as a reference.

Table 1. Composition of the steels used in wt.%.

Steel	Fe	Cr	Mn	Si	Ti	Al	Nb	W	Other
AISI 430*	Bal.	16.3	0.42	0.41	0.007	0.006	0.015	0.035	0.08 V, 0.076 Mo
AISI 441*	Bal.	17.53	0.40	0.59	0.172	0.07	0.41		
Crofer 22 H**	Bal.	23.0	0.44	0.25	0.1	0.01	0.5	1.9	0.07 La

*According to Optical Emission Spectroscopy analysis conducted by Force Technology, Denmark. **According to manufacturer's certificate, charge number 0002028042.

The oxidation kinetics of MCO coated and bare, pre-oxidized steels were studied in air at 650, 700 and 750 °C for 2000 h. Oxidation was carried out in a box furnace (stagnant conditions) with the samples suspended on an alumina rod. Every 250 h, the furnace was cooled (120 °C/h) to room temperature and the samples weighed on a scale with 0.01 mg accuracy (XS205, Mettler Toledo).

The sample microstructure and composition were characterized before and after oxidation in a scanning electron microscope (SEM, Zeiss Supra) equipped with an energy dispersive X-ray spectrometer (EDX, Noran System Six). The EDX data was collected at 15 kV and analyzed using NSS Software. For this purpose, the samples were cold-vacuum embedded in epoxy (Struers, Denmark), polished in successive steps down to 1 µm, and carbon coated. The thickness of the oxide scale was determined by measuring on at least five different SEM images taken from random locations of the sample. The width of each image was 41 µm. In order to minimize bias, a random grid was overlaid each image and the thickness measured along seven gridlines. The reported values are thus the average and standard deviation of at least 35 measurements. The thickness can alternatively be estimated by using image analysis to determine the total area of the oxide scale and dividing this by the width of the analyzed area. We found that the two methods resulted in comparable results (difference is within the given standard deviation).

3 Results

3.1 As-sintered MCO coating

Figure 1 shows cross sectional SEM images of the as-sintered (2h at 900 °C in air) MCO coating on the Crofer 22 H, 441 and 430 steels. The coating was ~15-30 µm thick and had a similar morphology/porosity on all three steels. The porosity of the coating was relatively high, as a result of the relatively mild sintering heat treatment. The oxide scale formed between the coating and steel consisted of mainly Cr and O in a ratio proportionate with Cr_2O_3 according to EDX analysis. The thickness of the

Cr_2O_3 scale was measured to 0.4±0.1 µm for MCO coated Crofer 22 H, 0.6±0.1 µm for MCO coated 441 and 0.5±0.1 µm for MCO coated 430. In case of MCO coated 430, Si-enrichment was detected between the steel and the Cr_2O_3 scale by EDX analysis. The volume of the Si-enriched area was too small compared to the expected EDX interaction volume (~1 µm) to obtain an accurate quantification, but based on previous reports, the Si-enrichment likely corresponds to SiO_2 [22]. The SiO_2 scale is visible in the SEM back scatter electron (BSE) image (Fig. 1) by its darker contrast compared to the alloy and Cr_2O_3.

In addition to thermal growth of an oxide scale, various precipitates within the steel bulk were observed. Bright contrast precipitates rich in Nb and W (1:1 at.% ratio according to EDX) were observed in the bulk of Crofer 22 H and 441. These precipitates have previously been identified as the Laves phase $(Fe,Cr)_2(Nb,W,Si)$ [38–40]. The amount of Laves phase precipitates was greatest for Crofer 22 H. The 441 steel had additionally some darker contrast precipitates in the steel bulk that were rich in Ti and N (1:1 at.% ratio), likely the nitride TiN [41,42]. In case of the 430 steel, dark contrast precipitates rich in Cr and N (2.2:1 at.% ratio) were identified along the steel grain boundaries.

SEM images of the non-coated (bare) steels after pre-oxidation in air at 900 °C for 2 h are shown in Figure 1. On all three steel the oxide scale consisted of an inner Cr and O rich area and an outer Mn, Cr and O rich area according to EDX analysis (not shown), indicating formation of Cr_2O_3 and $(Mn,Cr)_3O_4$, respectively. The total oxide scale thickness was 0.5±0.1 µm for Crofer 22 H, 0.7±0.1 µm for 441 and 0.6±0.1 µm for 430. Thus, in all cases, the oxide scale on the bare, pre-oxidized steels was slightly thicker than for the MCO coated samples after sintering under the same conditions. Precipitates within the steel bulk, as described above for the coated steels, were also observed in the bare steels after pre-oxidation.

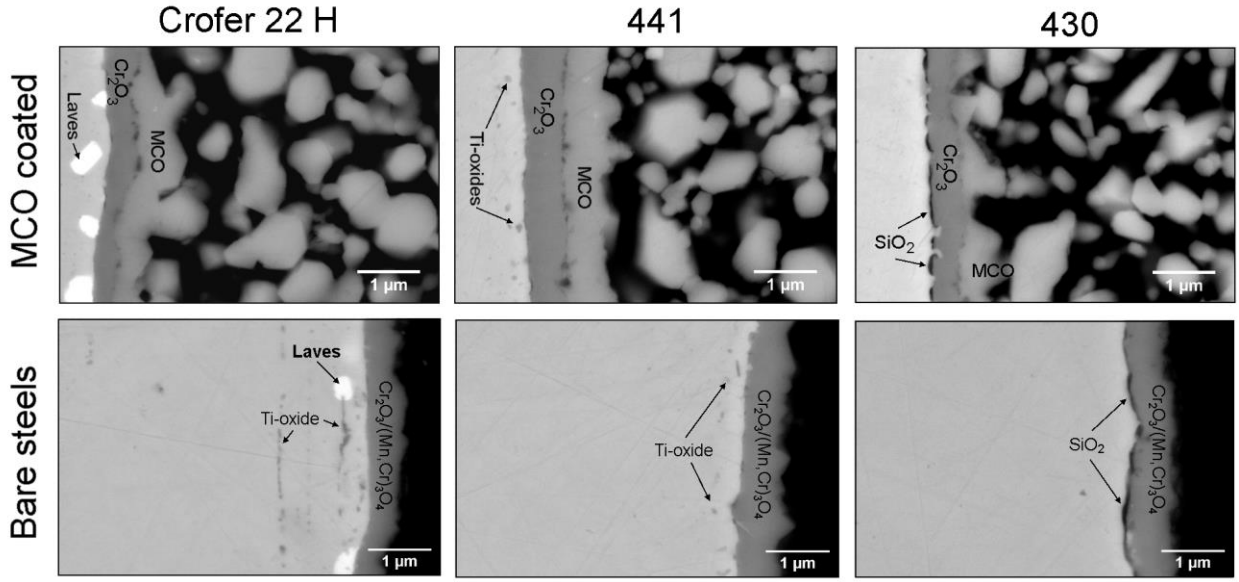

Figure 1. SEM cross sections of MCO coated steels after sintering and bare steels after pre-oxidation (2 h in air at 900 °C).

3.2 Oxidation kinetics

3.2.1 Oxidation at 650 °C

The mass change of the MCO coated and bare, pre-oxidized steels during oxidation in air at 650, 700 and 750 °C is shown in Figure 2. Each point is the average of five samples and the error bars give the standard deviation. Oxidation at 650 °C resulted in very small mass changes, close to the resolution of the scale (0.01 mg). This contributes to a large standard deviation, particularly for the MCO coated samples. For MCO coated Crofer 22 H and 430, the average mass change indicates a mass loss the first 1000-1200 h, followed by a mass gain up to 2000 h. For MCO coated 441 the mass changes were smaller, but also in this case there is a trend of increasing mass gain during the last 500 h of oxidation. In case of the bare, pre-oxidized steel (Fig. 2a), the mass remained nearly constant during the 2000 h of oxidation, with a weak trend for mass loss during the last 500 h of oxidation for all three steels.

3.2.1 Oxidation at 700 °C

Oxidation at 700 °C resulted in larger mass changes than at 650 °C. In case of uncoated Crofer 22 H, the mass increased during the first 750-1000 h of oxidation before it leveled off and started to decrease. In case of uncoated 441 and 430, the mass gain was nearly linear during the 2000 h of oxidation, with 441 showing an overall faster mass gain than 430 steel. A similar trend and magnitude of mass change was observed for the MCO coated 441 and 430 samples (Fig. 2d), i.e. the mass change measurement does not indicate any effect of the MCO coating for oxidation of 441 and 430 at 700 °C. In case of Crofer 22 H the MCO coating resulted in a larger mass loss than for the bare, pre-oxidized steel during oxidation at 700 °C. Since the mass loss is relatively small and continuous over 2000 h of oxidation, spallation of the coating can be ruled out.

3.2.1 Oxidation at 750 °C

The magnitude of the mass change increased further when the temperature was increased to 750 °C. The mass change of both the bare, pre-oxidized and the MCO coated samples followed a parabolic trend. That is, the mass change can be well fitted to the equation:

$$\left(\frac{\Delta m}{A}\right)^2 = k_p t \quad (1)$$

Where $\Delta m/A$ is the mass change per surface area (g cm^{-2}), t is the time (s) and k_p is the parabolic rate constant, summarized in Table 2. Comparing the mass change results for MCO coated and bare, pre-oxidized steels oxidized at 750 °C, indicates that the MCO coating reduced the oxidation rate of Crofer 22 H and 430 steels, but not of the 441 steel. It is also clear that a larger reduction in oxidation rate was achieved with the MCO coating on Crofer 22 H compared to on 430.

Table 2. Parabolic oxidation rate constant derived from mass change measured during oxidation in air at 750 °C.

	Bare steel [g^2 cm^{-4}s^{-1}]	MCO coated [g^2 cm^{-4}s^{-1}]
Crofer 22 H	3.2×10^{-15}	9.0×10^{-16}
441	1.1×10^{-14}	1.0×10^{-14}
430	4.7×10^{-15}	3.9×10^{-15}

During oxidation at all three temperatures, the standard deviation is larger on the coated samples compared to the uncoated. This may be due to inhomogeneity of the deposited coating among the different samples or, more likely, loss of small amounts of coating material during transportation and handling of the coated samples.

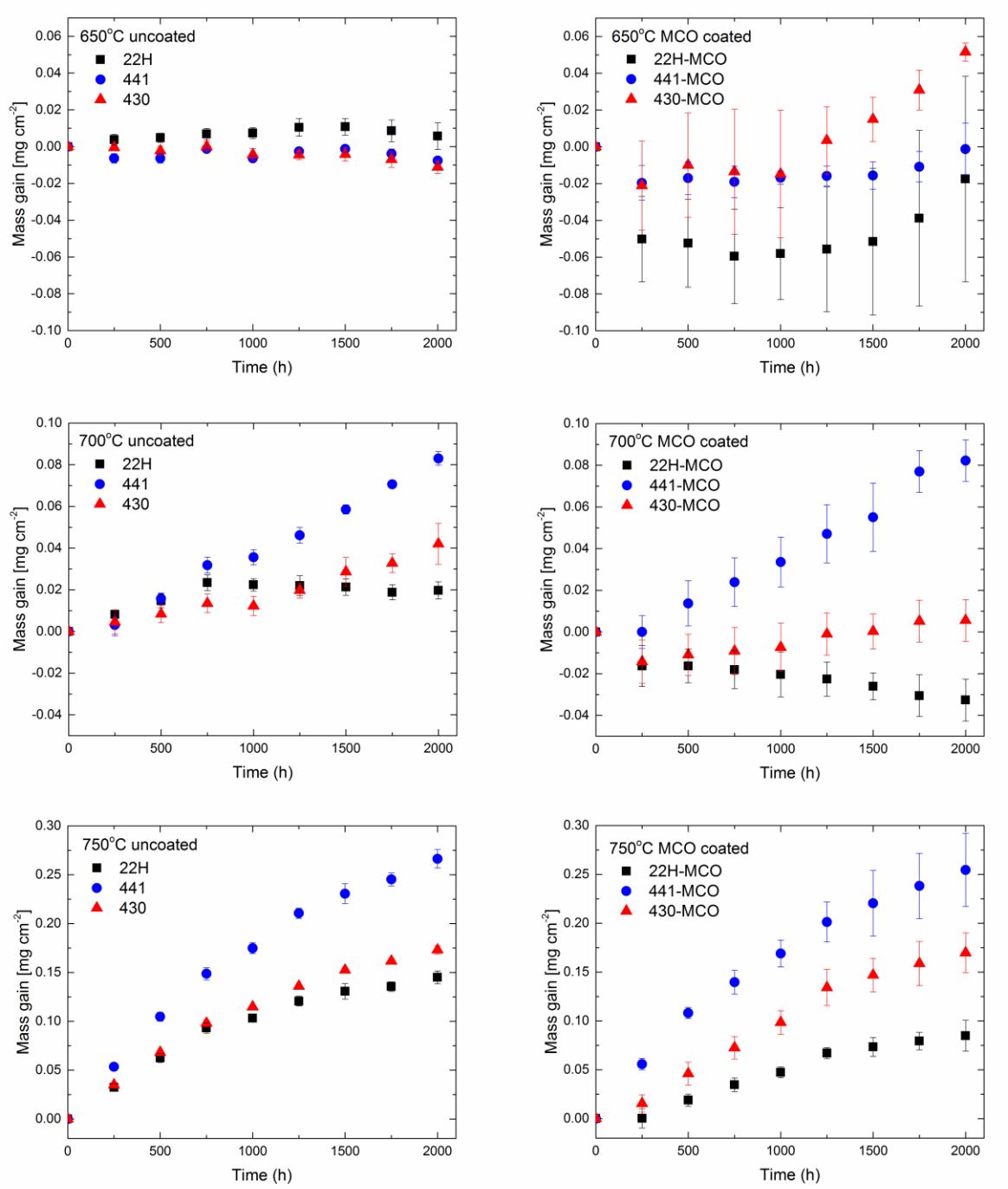

Figure 2. Mass gain during oxidation of bare and MCO coated Crofer 22 H, 441 and 430 at 650 °C, 700 °C and 750 °C in air. Each point is the average of five samples and the error bars show the standard deviation.

3.3. Microstructural characterization after oxidation

Cross sectional SEM images of the MCO coated and bare (pre-oxidized) steels after 2000 h of oxidation in air at 650 °C, 700 °C and 750 °C are shown in Figure 3, 4 and 5, respectively. On all three bare steels a duplex scale consisting of an outer $(Mn,Cr)_3O_4$ layer and an inner Cr_2O_3 layer was identified by EDX-analysis (not shown). On 441 and 430, the $(Mn,Cr)_3O_4$ is seen as faceted crystals on the surface, with a shape reflecting the cubic symmetry of the spinel structure. These crystals became more distinct with increasing temperature of oxidation. Their distribution on the surface did not appear to follow any obvious trend. On the MCO coated steels, the oxide scale formed between the alloy and the coating consisted of mainly Cr_2O_3 according to EDX analysis.

A SiO_2 scale was formed at the Cr_2O_3/steel interface on all three steels after oxidation. The scale was thickest on the 430 alloy, followed by 441 and then Crofer 22 H. The thickness of the SiO_2 scale increased with increasing oxidation temperature, but the scale remained discontinuous on both 441 and 430 after 2000 h oxidation at 650 °C and 700 °C. As highlighted in the image of the MCO coated 430 sample (Fig. 4), steel "pegs" disrupt the SiO_2 scale and provide a conduction path from the steel to the Cr_2O_3 scale. Such "pegs" were also observed on the bare 430 steel. After 2000 h oxidation at 750 °C the SiO_2 scale was nearly continuous on the 441 and 430 steels, while on Crofer 22 H it remained discontinuous after 2000 h oxidation at all three temperatures. Comparing the SEM images of the MCO coated and bare steels, the SiO_2 scale appears to be thinner and less continuous on the coated samples (Fig. 3-5). According to EDX, up to 0.5 wt.% of free Si remained in the steel bulk of all three alloys after oxidation. Thus, the SiO_2 scale may continue to grow and become more continuous with continued oxidation.

An internal oxidation zone of Ti-rich oxides was observed in the near-scale region of the 441 and Crofer 22 H steels, on both the MCO coated and bare samples. The depth of the internal oxidation zone extended further into the Crofer 22 H steel compared to the 441 steel and the Ti-oxides appeared more well-dispersed. On the 441 steel, Ti-enrichment was also detected at the Cr_2O_3/steel interface. Furthermore, several gaps and signs of delamination at the steel/Cr_2O_3 interface could be observed after oxidation of both MCO coated and bare 441. The amount of other steel-bulk precipitates, i.e. Laves phase, Ti-nitrides and Cr-nitrides, did not change noticeably compared to after pre-oxidation/coating sintering (see Section 3.1).

In accordance with the mass change results, the oxide scales were overall thicker when the oxidation temperature was increased from 650 °C to 750 °C, both on the MCO coated and the bare steels. The average thickness of the oxide scales after 2000 h of oxidation is summarized in Figure 6 and was determined by measurements on at least five SEM images taken at different locations of the sample. According to these measurements the MCO coating reduces the oxide scale growth on all three steels at 700 °C and 750 °C, which was not apparent from the mass gain measurement (Fig. 2). In line with the mass gain results, measurements of the oxide scale thickness show that the beneficial effect of the coating increases with increasing temperature of oxidation, and that the greatest benefit is on the Crofer 22 H steel. At 650 °C there was no significant change in oxide scale thickness after 2000 h of oxidation compared to after pre-oxidation/sintering for any of the steels, as can be expected from the very low mass gain (Fig. 2).

Figure 7 shows EDX linescans of the MCO coated steels after 2000 h oxidation at 700 °C. A reaction/diffusion layer, consisting of Mn, Co, Cr and Fe was formed between the Cr_2O_3 scale and the coating. This reaction layer was clearly thicker and more distinct for the MCO coated Crofer 22 H and 430 steels than on the 441 steel. The diffusion of Cr and Fe from the steel has led to partial densification of the coating in the vicinity of the scale/coating interface. Areas where significant amounts (>5 wt.%) of Cr were detected in the coating have been annotated as "MCO+Cr" in Figures 3-5. As apparent from these SEM images, the densification due to diffusion of Cr and Fe became more pronounced with increasing temperature of oxidation. However, the reaction layer was not continuous even after 2000 h of oxidation at 750 °C.

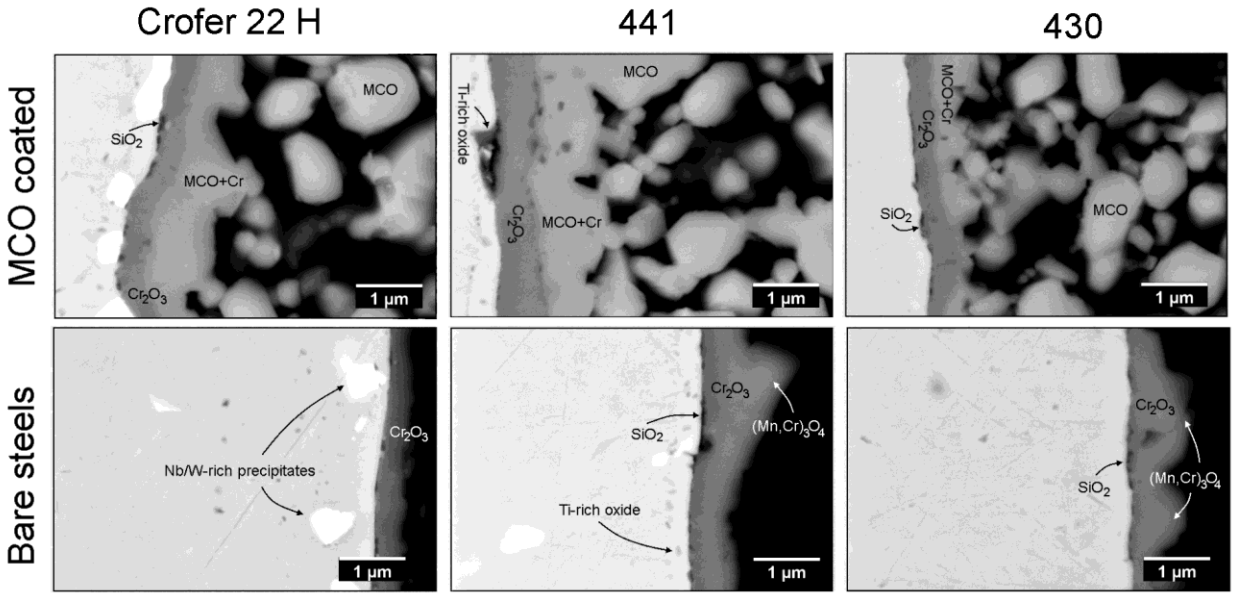

Figure 3. SEM cross sections of bare (pre-oxidized) and MCO coated steels after 2000 h oxidation at 650 °C

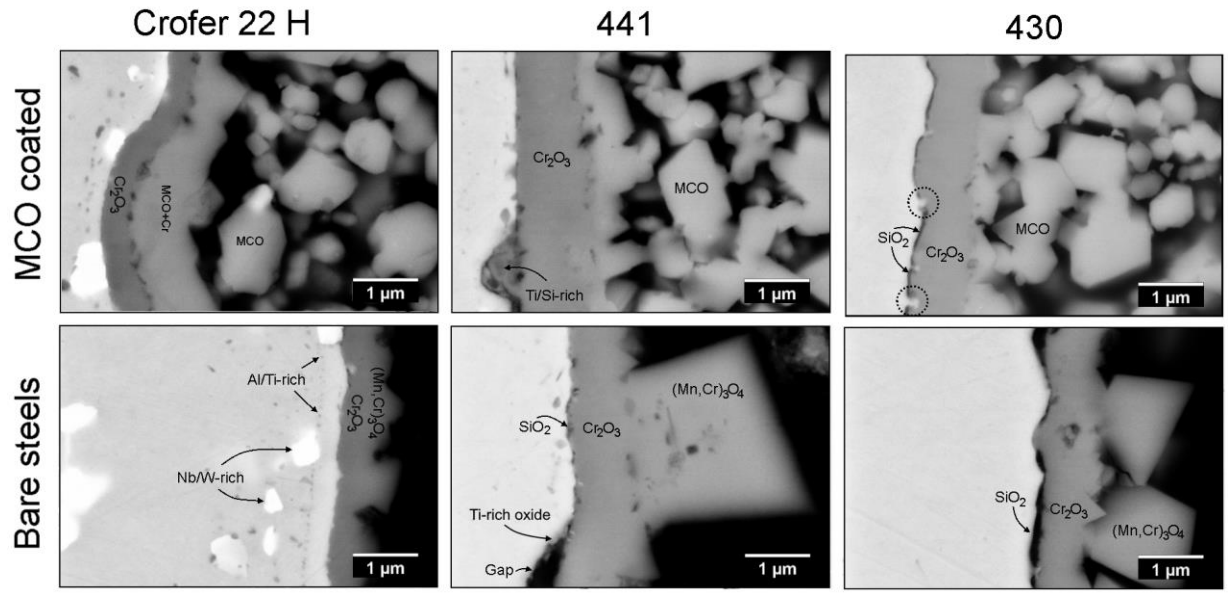

Figure 4. SEM cross sections of bare (pre-oxidized) and MCO coated steels after 2000 h oxidation at 700 °C

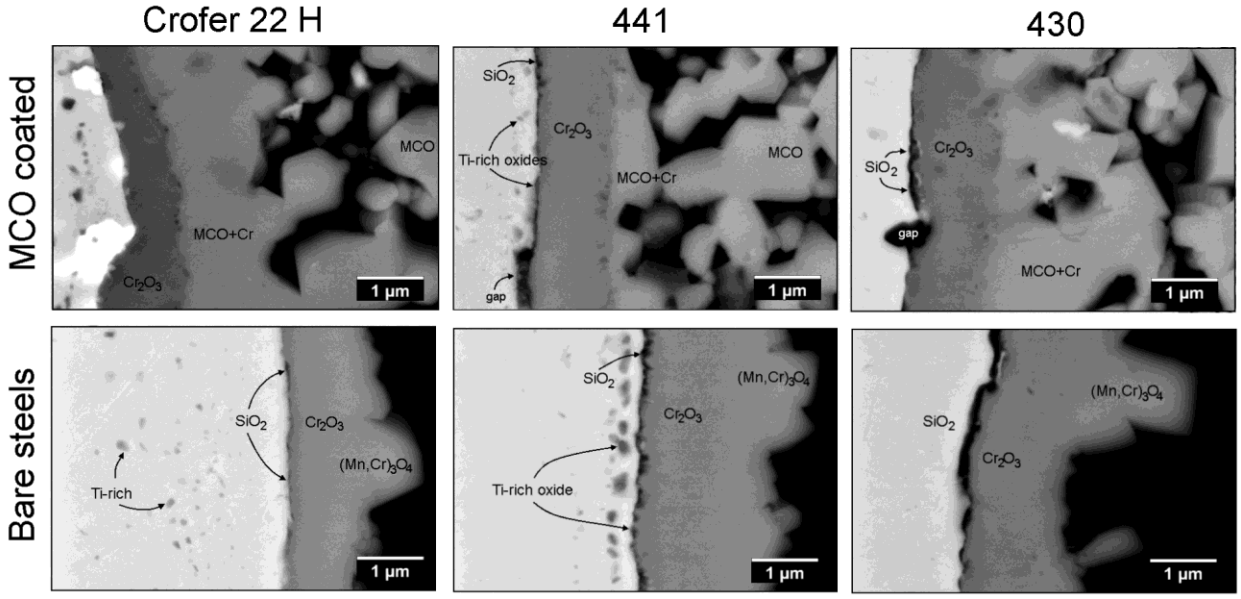

Figure 5. SEM cross sections of bare (pre-oxidized) and MCO coated steels after 2000 h oxidation at 750 °C

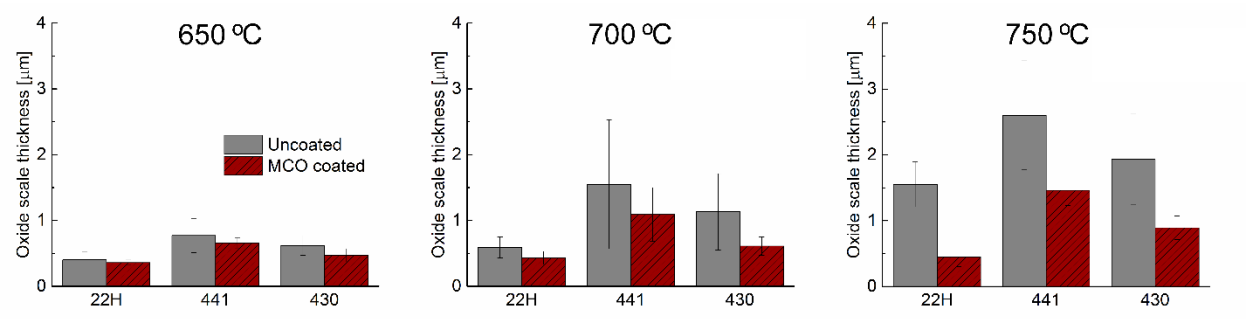

Figure 6. Oxide scale thickness measured on SEM cross sections of samples oxidized 2000 h in air at 650, 700 and 750 °C.

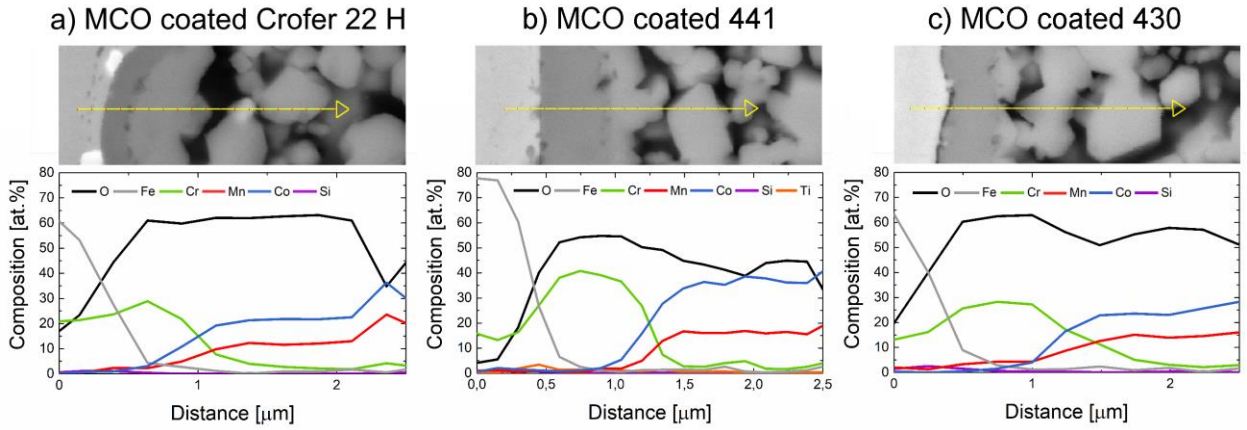

Figure 7. EDX linescans of MCO coated Crofer 22 H (a), 441 (b) and 430 (c) after 2000 h of oxidation at 700 °C. The length of the arrow in the micrographs is 2.5 µm.

X-ray diffractograms of the samples after 2000 h of oxidation at 750 °C are shown in Figure 8. The diffractograms are representative also for samples oxidized at 700 and 650 °C, except for small differences in the relative intensity of the peaks belonging to the different phases. The increasing background with increasing 2θ angle is due to fluorescence of Fe (in the steel) and Co (in the MCO coating). For the bare steels, peaks belonging to the two oxides Cr_2O_3 and $(Mn,Cr)_3O_4$ spinel are detected in addition to peaks from the ferritic stainless steel. Bare Crofer 22 APU has some additional peaks (highlighted in Fig. 8a), which could not be properly indexed, but possibly belong to the Laves phase $(Fe,Cr)_2(Nb,W,Si)$. For the MCO coated samples, all peaks can be indexed to the $MnCo_2O_4$ cubic spinel oxide.

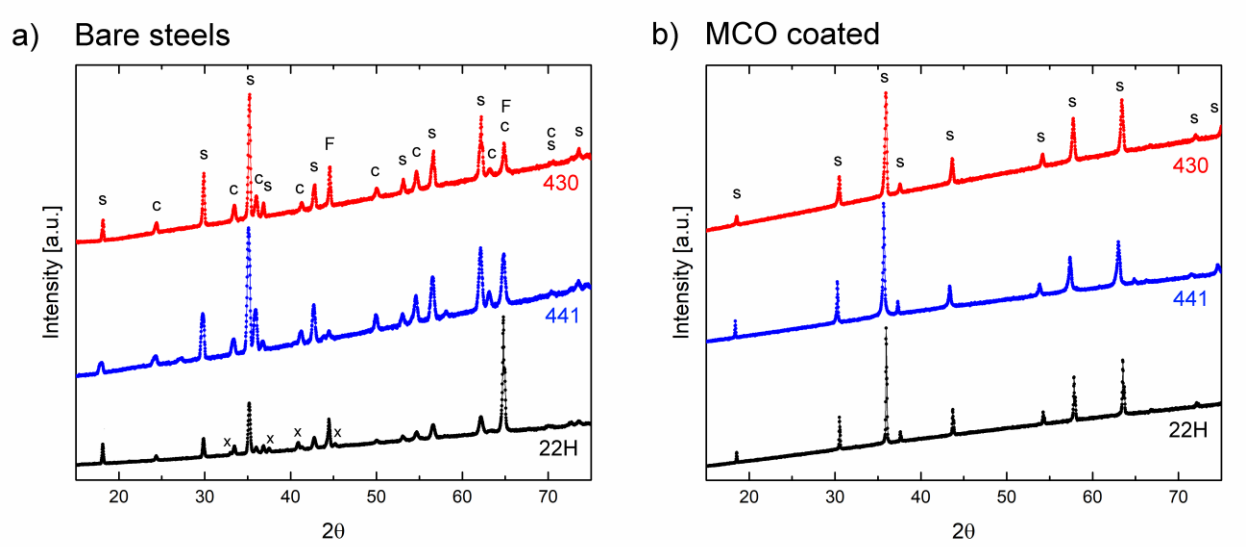

Figure 8. X-ray diffractograms of samples after 2000 h of oxidation at 750 °C. Individual patterns are normalized to the highest intensity peak. a) Bare steels, with the symbols identify peaks belonging to: (s) $(Mn,Cr)_3O_4$ cubic spinel oxide (c) Cr_2O_3, (F) the ferritic stainless steel substrate, and (x) unindexed peaks. b) MCO coated steels, with the symbol (s) identifying peaks belonging to a cubic $MnCo_2O_4$ spinel.

4 Discussion

4.1 Oxidation behavior of bare steels

4.1.1 Influence of temperature and pre-treatment

It is well-established that the growth rate of oxide scales on FeCr-alloys generally decreases with decreasing temperature [43], which was also observed here. At 750 °C the oxidation kinetics followed a parabolic trend, while at lower temperature (650-700 °C) the kinetics appeared more time-invariant. Some of the steels even displayed a mass loss after the first 500-1000 h of exposure. This behavior (mas gain followed by mass loss) is characteristic of oxidation kinetics governed by a combination of diffusion controlled (parabolic) oxide scale growth and linear (time invariant) oxide scale evaporation [43,44]. Under this regime, the oxide scale grows until a certain thickness is reached where evaporation and oxidation proceed at the same rate. With continued aging the thickness of the oxide scale will remain invariant, but a mass loss will be recorded. The activation energy for Cr-vaporization is lower than the activation energy for oxidation, thus, Cr vaporization has a relatively larger influence on the mass change at lower oxidation temperatures [36,45].

When the temperature is decreased below a certain limit, the oxidation rate may start to increase again due to formation of faster growing Fe-oxides instead of the more protective Cr_2O_3. Young et al. [46] reported that for Crofer 22 APU oxidized in Ar-4%H_2-20%H_2O atmosphere, the transition from a protective Cr_2O_3 scale to the formation of non-protective Fe-oxides is at 650 °C. Falk-Windisch et al. [33] observed Fe-containing oxides forming on Co-coated Sanergy HT after oxidation in air-3%H_2O at 650 °C. Here, we only observe the very slow growth of Cr_2O_3 and $(Mn,Cr)_3O_4$ at all three temperatures. It is most likely the pre-oxidation carried out at 900 °C that results in the low oxidation rate during

subsequent aging at lower temperature [47]. Also in [33] the formation of Fe-oxides on Co coated Sanergy HT at 650 °C was avoided by pre-oxidizing the samples at 900 °C for 3 min.

4.1.2 Influence of steel composition

The differences in oxidation rate and oxide scale morphology for the three steels may be explained by comparing the chemical compositions, given in Table 1. Crofer 22 H contains La, which is a reactive element (RE) known to improve the oxidation resistance of FSS [15,48]. The mechanism responsible for the beneficial effect of RE is not well understood, but several observations point to a reduced oxidation rate, improved scale adherence and reduced growth stresses [15,49,50]. It has been suggested that RE additions change the growth mechanism of the oxide scale from being dominated by cation outward diffusion (no RE), where the oxide scale grows at the scale/air interface, to being dominated by oxide ion inward diffusion (with RE), where the oxide scale grows at the scale/steel interface [51–53].

Although the oxide scale growth on both Crofer 22 H (with RE) and 441/430 (no RE) most likely proceeds by a combination of the two mechanisms, the morphology of the oxide scales suggests different mechanisms prevail for the two types of steels. The formation of faceted oxide crystals in case of 441/430 suggests that the oxide scale is more dominated by outwards transport of cations (Cr+Mn) compared to the oxide scale grown on Crofer 22 H, which is generally more smooth. Furthermore, gaps observed along the oxide scale and 441/430 interface points to a mechanism involving vacancy condensation or outward diffusion of interstitial metal cations [54].

The higher oxidation rate of 441 compared to 430 may in part be related to the high Ti content of the former (0.172 wt.%). Ti is typically added as an alloying element to increase the austenitization temperature (by locking up the free N and C) and/or to stabilize the Laves phase (by increases the solvus temperature) [40]. It has been suggested that Ti additions also may increase the steel oxidation rate due to Ti doping of the Cr_2O_3 scale [55–57]. Depending on the local partial pressure of oxygen within the Cr_2O_3 scale, which decreases from the scale/air interface to the scale/steel interface, doping with Ti^{4+} will be compensated by the creation of chromium vacancies or electrons, respectively [55]. The increase of chromium vacancies increases the diffusion rate of Cr^{3+} from the scale/steel interface to the scale/air interface, which consequentially increases the oxidation rate of the steel. It has been postulated that Nb^{4+}/Nb^{5+} doping of Cr_2O_3 may increase the oxide scale growth rate according to the same mechanism as Ti-doping [38]. Nb is added as an alloying element to Crofer 22 H and 441, and is only found as a trace element/impurity in 430.

4.1.3 Laves phase precipitation and the formation of silica subscales

The chemical composition differences between the three steels may also explain the differences in thickness of the silica scales and the concentration of Laves phase precipitates. Compared to 441, Crofer 22 H has a lower Si content, higher Nb content, and additions of W. Both Nb and W promote Laves phase formation [58,59], accordingly, the volume of the Laves phase precipitates in Crofer 22 H is greater than in 441. As the Laves phase incorporates Si, the concentration of free Si in the alloy matrix is reduced to a lower level in Crofer 22 H than in 441, and consequentially, a thinner silica scale is formed. The same argument can be used to explain why a thinner silica scale is formed on 441 compared to 430, despite the higher Si content in the former (0.59 vs 0.41 wt.%, respectively).

One might imagine that the formation of SiO_2 can be completely avoided by optimizing the ratio between Si and Nb/W. Alas, this approach has proven difficult [33,35]. Jablonski et el. [40] estimated that for 441 with a nominal Si content of 0.34 wt.%, 0.5 wt.% of Nb and 0.22 wt.% of Ti, 0.23 wt.% of the Si remain dissolved in the steel matrix after the Laves phase has formed. After oxidizing this steel for 2000 h at 800 °C they observed discontinuous regions with Si-enrichment along the steel/Cr_2O_3 interface. The Crofer 22 H used in the current work contains even less Si (0.25wt.%) and a greater total amount of the elements promoting Laves phase formation (Nb, W, Ti), yet, a discontinuous silica scale is formed after 2000 h oxidation at 650-750 °C.

The formation of a silica scale on interconnect alloys is generally undesired due to the high electrical resistivity of this oxide. As highlighted in Figure 4, the SiO_2 layer is penetrated by multiple steel "pegs" that connect the steel to the chromia scale. These pegs will serve as paths of high electrical conductivity, thus lowering the area specific resistance (ASR) across the interconnect [60]. Therefore, as long as the silica scale remains discontinuous, it will not influence the interconnect ASR noticeably. This should be further confirmed by measuring the ASR of the three steels at the relevant temperature.

4.1.4 Oxide scale adhesion

Another and even more detrimental effect of the formation of a silica scale is the increased risk for spallation [28,61], which may lead to contact losses and a decreased component lifetime. Here, no spallation of the oxide scale was observed after oxidation at 650-750 °C for 2000 h, although SEM inspection after oxidation revealed gaps between the oxide scale and steel, indicating a weak interface. The lower oxidation temperature and to a lesser degree also the relatively slow cooling rate (120 °C h^{-1}) used for the cyclic oxidation tests may explain why no spallation was observed despite the interface weakness. Spallation of oxide scales typically occurs during thermal cycling due to the stresses developed from the thermal expansion mismatch between the oxide scale and the steel [62]. Using a much faster cooling rate (300 °C min^{-1}) Belogolovsky et al. [63] reported that the time to oxide spallation of 430 oxidized at 750 °C was only 100 h. However, by decreasing the temperature from 750 to 600 °C the time to oxide spallation increased by at least three orders of magnitude, due to a combined effect of lower thermal stresses and the slower oxide scale growth rate [63]. This means that for a low operating temperature of 650 °C, oxide scale spallation due to SiO_2 formation does not seem to limit the interconnect lifetime.

A contributing reason for the poor scale adhesion on 441 can be attributed to the Ti additions. As discussed in Section 4.1.2, Ti is believed to increase the diffusion rate of Cr^{3+} in the Cr_2O_3 scale. If the diffusion rate in the scale is faster than the diffusion rate of Cr^{3+} in the steel, the concentration of cation vacancies at the steel/oxide scale interface will increase, effectively forming a gap. Furthermore, the volume change associated with the formation of Ti-oxides near the steel/oxide scale interface may lead to disruption of the protective scale and increase the risk of spallation. Accordingly, a promising way to improve the oxide scale adhesion on 441 could be to decrease the level of Ti. Others have suggested that the oxide scale adhesion on 441 steel can be improved by sandblasting [63,64], as the increased surface roughness makes crack propagation along the oxide scale/steel interface more difficult.

4.2 Protective effect of MCO coating

The thickness of the spinel coating deposited on the three steels varied between 15-30 µm, but this had likely no significant influence on the results. Molin et al. [19] found no differences in ASR or corrosion rate between Crofer 22 APU with a 30 µm thick and a 50 µm thick MCO coating. The relatively mild sintering conditions (900 °C in air) resulted in a porous coating, as expected based on previous work on sintering of MCO coatings [17,37]. It has been shown that a higher coating density can be achieved if the coating is first sintered in a reducing atmosphere and then in air [17,24,37,65,66]. However, this two-step sintering procedure adds to the costs of the coating process. According to some estimates, sintering of the MCO coating can amount as much as 20 % of the total coating costs [67,68]. Thus, a single step sintering process in air would lead to cost savings in a commercial production line. As the aim of this work was to find low-cost alternatives for coated interconnects, the sintering step in reducing atmosphere was omitted. We have previously shown that even a highly porous MCO coating (sintered in air at 900 °C) reduces the oxidation rate and Cr vaporization of Crofer 22 APU at 800 °C, although a denser coating is even more protective [17]. Here, we evaluate whether the single step-sintering method is suitable on cheaper steels at lower operating temperatures (650-750 °C).

The oxide scale thickness measurements (Fig. 6) show that the MCO coating reduces the oxidation rate of all three steels at 750 and 700 °C, and that that the difference between the coated and bare steel decreases with decreasing temperature. In Ref. [10] we showed that an initially highly porous spinel coating on Crofer 22 APU, resulting from sintering in air at 900 °C, densified with time during aging. After 2000 h oxidation at 800 °C the Cr_2O_3 scale was covered by a continuous layer of $(Mn,Co,Cr)_3O_4$, due to interactions between the steel and the coating. Here, the MCO coating is visibly denser after oxidation also at the lower temperatures of 650-750 °C, but the reaction layer is considerably thinner and does not completely cover the chromia scale. An incomplete coverage of the chromia scale will lead to higher Cr vaporization rates due to the direct exposure of chromia to the oxidizing atmosphere. Based on these observations it may be concluded that the cheaper sintering treatment (air treatment only) is less suitable for interconnects intended for low temperature operation (<800 °C). Another approach to increase the coating density for low temperature applications, besides introducing a high temperature reduction heat treatment step, could be to infiltrate the porous MCO coating with Co and Mn nitrites, as suggested by Molin et al. [12].

According to the oxidation results and inspections of the oxide scale thickness, the MCO coating provides greater protection on steels that have a lower mass gain when not coated, that is, the coating has a greater effect on Crofer 22 H than on 441 and 430. These observations may be related to the different mechanisms by which the oxide scale grows on the three steels. As discussed in Section 4.1.2, literature and the result in this work suggest that the oxide scale on Crofer 22 H grows by predominant oxygen ion transport while the oxide scales on 441 and 430 grow by predominant metal cation outward diffusion. The MCO coating is believed to reduce the oxidation rate of steel by limiting the transport of oxygen to the oxide scale surface and forming a reaction layer with relatively slow transport [69]. In case of Crofer 22 H, the reduced access of O_2 reduces the oxidation rate, while for 441 and 430, the reduction is smaller as the oxidation rate is more dominated by the diffusion rate of cations through the growing oxide scale. It should be emphasized that this model is a simplification of the oxidation process, which likely involves a complicated mixture of both anion and cation diffusion in the oxide scale bulk and grain boundaries for both types of steel.

4.3 Possibilities and limitations of low-cost steels.

Considering only the oxidation resistance, the results show that a mild pre-oxidation heat treatment may provide sufficient "protection" at 650 °C to enable the use of the low-cost steels 441 and 430. However, pre-oxidation will not protect against Cr vaporization, which is still prominent at 650 °C [42,43]. Therefore, although pre-oxidation is sufficient to provide an acceptable oxidation resistance at 650 °C, a protective coating is necessary to prevent Cr poisoning of the oxygen/air electrode. The MCO coating has previously been shown to be very effective for this purpose [17,70,71]. However, for operating temperatures < 750 °C it is recommended to pre-densify the MCO coating by a two-step reduction and re-oxidation procedure as the amount of in-situ densification is limited at low temperatures.

The result in this work show that the MCO coating can be used to improve the oxidation resistance of low-cost steels such as 441 and 430. Nevertheless, the coating appears to be more effective on Crofer 22 H. As discussed above, this is attributed to the difference in the oxidation mechanism of the Crofer 22 H and 441/430 steels, which is an effect of the La additions in Crofer 22 H. The La is added to the Crofer 22 H melt during production, but La or other REs may also be applied to the steel surface in the form of a coating [23,72]. This may be a cheaper option, as the amount of RE needed are reduced and the difficulties with adding RE to the melt (reactions with the crucible) are avoided. Coating the 441 and 430 steels with RE should aid to both decrease the growth rate of the chromia scale and improve scale adherence [23,63,72,73]. The combination of MCO and Ce on 441 has already been shown to improve the oxide scale adhesion and reduce the presence of micro-gaps at the oxide scale/steel interface after oxidation at 800 °C [24]. However, this solution remains to be proven for lower temperature applications.

5 Conclusion

The protective effect of a $MnCo_2O_4$ (MCO) coating on Crofer 22 H, 430 and 441 steels was investigated by oxidation in air at 650, 700 and 750 °C. The MCO coating reduced the oxide scale thickness on all three steels during oxidation in air at 700-750 °C, while at 650 °C the low oxidation rate of the bare, pre-oxidized steel, made it difficult to evaluate the protective effect of the MCO coating. The highest protective effect, in terms of reduced oxide scale thickness relative to the uncoated steel, was found for Crofer 22 H. The differences between the MCO coated and bare, pre-oxidized steels became more prominent with increasing temperature of oxidation.

A SiO_2 scale was formed at the Cr_2O_3/steel interface of all three steel after oxidation at 650-750 °C. The thickness of the SiO_2 scale increased with increasing temperature of oxidation, but the scale remained discontinuous after 2000 h and should therefore not have a major influence on the resistance across interconnect. For lower operating temperatures (650-700 °C), the MCO coating and a suitable pre-treatment provided sufficient protection to make the low-cost steels 441 and 430 promising interconnect materials. At higher temperatures (750 °C), the 441 steel suffered from poor oxide scale adhesion, making it unattractive as the interconnect material.

Acknowledgement
Financial support from EUDP (Danish Energy Agency) project 64012-0225 “SOFC Accelerated – Development to Accelerate Field Demonstrations” is gratefully acknowledged.

Declarations of interest: none

References

[1] Huijsmans JPP, van Berkel FPF, Christie GM. Intermediate temperature SOFC – a promise for the 21st century. J Power Sources 1998;71:107–10. https://doi.org/10.1016/S0378-7753(97)02789-4.
[2] L. Brett DJ, Atkinson A, P. Brandon N, J. Skinner S. Intermediate temperature solid oxide fuel cells. Chem Soc Rev 2008;37:1568–78. https://doi.org/10.1039/B612060C.
[3] Kofstad P, Bredesen R. High temperature corrosion in SOFC environments. Solid State Ion 1992;52:69–75. https://doi.org/10.1016/0167-2738(92)90092-4.
[4] Linderoth S, Hendriksen PV, Mogensen M, Langvad N. Investigations of metallic alloys for use as interconnects in solid oxide fuel cell stacks. J Mater Sci 1996;31:5077–82. https://doi.org/10.1007/BF00355908.
[5] Quadakkers WJ, Prion-Abellan J, Shemet V, Singheiser L. Metallic interconnectors for solid oxide fuel cells – a review. Mater High Temp 2003;20:115–27.
[6] Zhu WZ, Deevi SC. Opportunity of metallic interconnects for solid oxide fuel cells: a status on contact resistance. Mater Res Bull 2003;38:957–72. https://doi.org/10.1016/S0025-5408(03)00076-X.
[7] Huczkowski P, Ertl S, Piron-Abellan J, Christiansen N, Höfler T, Shemet V, et al. Effect of component thickness on lifetime and oxidation rate of chromia forming ferritic steels in low and high pO2 environments. Mater High Temp 2005;22:253–62. https://doi.org/10.1179/mht.2005.029.
[8] Sachitanand R, Svensson J-E, Froitzheim J. The Influence of Cr Evaporation on Long Term Cr Depletion Rates in Ferritic Stainless Steels. Oxid Met 2015;84:241–57. https://doi.org/10.1007/s11085-015-9552-5.
[9] Hilpert K, Das D, Miller M, Peck DH, Weiß R. Chromium Vapor Species over Solid Oxide Fuel Cell Interconnect Materials and Their Potential for Degradation Processes. J Electrochem Soc 1996;143:3642–7. https://doi.org/10.1149/1.1837264.
[10] Yokokawa H, Horita T, Sakai N, Yamaji K, Brito ME, Xiong Y-P, et al. Thermodynamic considerations on Cr poisoning in SOFC cathodes. Solid State Ion 2006;177:3193–8. https://doi.org/10.1016/j.ssi.2006.07.055.
[11] Bentzen JJ, Høgh JVT, Barfod R, Hagen A. Chromium Poisoning of LSM/YSZ and LSCF/CGO Composite Cathodes. Fuel Cells 2009;9:823–32. https://doi.org/10.1002/fuce.200800143.
[12] Huczkowski P, Shemet V, Piron-Abellan J, Singheiser L, Quadakkers WJ, Christiansen N. Oxidation limited life times of chromia forming ferritic steels. Mater Corros 2004;55:825–30. https://doi.org/10.1002/maco.200303798.
[13] Stanislowski M, Wessel E, Hilpert K, Markus T, Singheiser L. Chromium Vaporization from High-Temperature Alloys I. Chromia-Forming Steels and the Influence of Outer Oxide Layers. J Electrochem Soc 2007;154:A295–306. https://doi.org/10.1149/1.2434690.

[14] Alman DE, Jablonski PD. Effect of minor elements and a Ce surface treatment on the oxidation behavior of an Fe–22Cr–0.5Mn (Crofer 22 APU) ferritic stainless steel. Int J Hydrog Energy 2007;32:3743–53. https://doi.org/10.1016/j.ijhydene.2006.08.032.
[15] Hou PY, Stringer J. The effect of reactive element additions on the selective oxidation, growth and adhesion of chromia scales. Mater Sci Eng A 1995;202:1–10. https://doi.org/10.1016/0921-5093(95)09798-8.
[16] Sachitanand R, Sattari M, Svensson J-E, Froitzheim J. Evaluation of the oxidation and Cr evaporation properties of selected FeCr alloys used as SOFC interconnects. Int J Hydrog Energy 2013;38:15328–34. https://doi.org/10.1016/j.ijhydene.2013.09.044.
[17] Talic B, Falk-Windisch H, Venkatachalam V, Hendriksen PV, Wiik K, Lein HL. Effect of coating density on oxidation resistance and Cr vaporization from solid oxide fuel cell interconnects. J Power Sources 2017;354:57–67. https://doi.org/10.1016/j.jpowsour.2017.04.023.
[18] Talic B, Molin S, Wiik K, Hendriksen PV, Lein HL. Comparison of iron and copper doped manganese cobalt spinel oxides as protective coatings for solid oxide fuel cell interconnects. J Power Sources 2017;372:145–56. https://doi.org/10.1016/j.jpowsour.2017.10.060.
[19] Molin S, Jasinski P, Mikkelsen L, Zhang W, Chen M, Hendriksen PV. Low temperature processed $MnCo_2O_4$ and $MnCo_{1.8}Fe_{0.2}O_4$ as effective protective coatings for solid oxide fuel cell interconnects at 750 °C. J Power Sources 2016;336:408–18. https://doi.org/10.1016/j.jpowsour.2016.11.011.
[20] Froitzheim J, Canovic S, Nikumaa M, Sachitanand R, Johansson LG, Svensson JE. Long term study of Cr evaporation and high temperature corrosion behaviour of Co coated ferritic steel for solid oxide fuel cell interconnects. J Power Sources 2012;220:217–27. https://doi.org/10.1016/j.jpowsour.2012.06.092.
[21] Larring Y, Norby T. Spinel and Perovskite Functional Layers Between Plansee Metallic Interconnect (Cr-5 wt % Fe-1 wt % Y_2O_3) and Ceramic $(La_{0.85}Sr_{0.15})_{0.91}MnO_3$ Cathode Materials for Solid Oxide Fuel Cells. J Electrochem Soc 2000;147:3251–6. https://doi.org/10.1149/1.1393891.
[22] Jablonski PD, Sears JS. The impact of alloy chemistry on the formation of a silicon-rich subscale on two classes of ferritic steels. J Power Sources 2013;228:141–50. https://doi.org/10.1016/j.jpowsour.2012.11.107.
[23] Grolig JG, Froitzheim J, Svensson J-E. Coated stainless steel 441 as interconnect material for solid oxide fuel cells: Oxidation performance and chromium evaporation. J Power Sources 2014;248:1007–13. https://doi.org/10.1016/j.jpowsour.2013.08.089.
[24] Stevenson JW, Yang ZG, Xia GG, Nie Z, Templeton JD. Long-term oxidation behavior of spinel-coated ferritic stainless steel for solid oxide fuel cell interconnect applications. J Power Sources 2013;231:256–63. https://doi.org/10.1016/j.jpowsour.2013.01.033.
[25] Huang J-J, Li C, Lee S, Li Y-S. Experimental assessments on the resistance to oxidation and Cr evaporation of several Fe–Cr based alloys. Intermetallics 2013;43:162–70. https://doi.org/10.1016/j.intermet.2013.07.016.
[26] Ebrahimifar H, Zandrahimi M. Influence of oxide scale thickness on electrical conductivity of coated AISI 430 steel for use as interconnect in solid oxide fuel cells. Ionics 2012;18:615–24. https://doi.org/10.1007/s11581-012-0664-5.
[27] Hua B, Pu J, Gong W, Zhang J, Lu F, Jian L. Cyclic oxidation of Mn–Co spinel coated SUS 430 alloy in the cathodic atmosphere of solid oxide fuel cells. J Power Sources 2008;185:419–22. https://doi.org/10.1016/j.jpowsour.2008.06.055.

[28] Chandra-Ambhorn S, Wouters Y, Antoni L, Toscan F, Galerie A. Adhesion of oxide scales grown on ferritic stainless steels in solid oxide fuel cells temperature and atmosphere conditions. J Power Sources 2007;171:688–95. https://doi.org/10.1016/j.jpowsour.2007.06.058.
[29] Yang Z, Xia G-G, Wang C-M, Nie Z, Templeton J, Stevenson JW, et al. Investigation of iron–chromium–niobium–titanium ferritic stainless steel for solid oxide fuel cell interconnect applications. J Power Sources 2008;183:660–7. https://doi.org/10.1016/j.jpowsour.2008.05.037.
[30] Jia C, Wang Y, Molin S, Zhang Y, Chen M, Han M. High temperature oxidation behavior of SUS430 SOFC interconnects with Mn-Co spinel coating in air. J Alloys Compd 2019;787:1327–35. https://doi.org/10.1016/j.jallcom.2019.01.015.
[31] Lv Y, Geng S, Shi Z. Evaluation of electroplated copper coating on ferritic stainless steel for solid oxide fuel cells interconnects. J Alloys Compd 2017;726:269–75. https://doi.org/10.1016/j.jallcom.2017.07.318.
[32] Shao Y, Guo PY, Sun H, Zhou TC, Ding JT, Xu KX, et al. Structure and properties of composite Ni–Co–Mn coatings on metal interconnects by electrodeposition. J Alloys Compd 2019:152006. https://doi.org/10.1016/j.jallcom.2019.152006.
[33] Falk-Windisch H, Claquesin J, Sattari M, Svensson J-E, Froitzheim J. Co- and Ce/Co-coated ferritic stainless steel as interconnect material for Intermediate Temperature Solid Oxide Fuel Cells. J Power Sources 2017;343:1–10. https://doi.org/10.1016/j.jpowsour.2017.01.045.
[34] Jian P, Jian L, Bing H, Xie G. Oxidation kinetics and phase evolution of a Fe–16Cr alloy in simulated SOFC cathode atmosphere. J Power Sources 2006;158:354–60. https://doi.org/10.1016/j.jpowsour.2005.09.056.
[35] Windisch HF, Svensson J-E, Froitzheim J. Metallic Thin-Film Co- and Ce/Co-Coated Steels as Interconnect Material in IT-SOFC. ECS Trans 2017;78:1607–14. https://doi.org/10.1149/07801.1607ecst.
[36] Falk-Windisch H, Svensson JE, Froitzheim J. The effect of temperature on chromium vaporization and oxide scale growth on interconnect steels for Solid Oxide Fuel Cells. J Power Sources 2015;287:25–35. https://doi.org/10.1016/j.jpowsour.2015.04.040.
[37] Bobruk M, Molin S, Chen M, Brylewski T, Hendriksen PV. Sintering of MnCo 2 O 4 coatings prepared by electrophoretic deposition. Mater Lett 2018;213:394–8. https://doi.org/10.1016/j.matlet.2017.12.046.
[38] Froitzheim J, Meier GH, Niewolak L, Ennis PJ, Hattendorf H, Singheiser L, et al. Development of high strength ferritic steel for interconnect application in SOFCs. J Power Sources 2008;178:163–73. https://doi.org/10.1016/j.jpowsour.2007.12.028.
[39] Yamamoto K, Kimura Y, Mishima Y. Effect of matrix microstructure on precipitation of Laves phase in Fe–10Cr–1.4W(–Co) alloys. Intermetallics 2006;14:515–20. https://doi.org/10.1016/j.intermet.2005.09.005.
[40] Jablonski PD, Cowen CJ, Sears JS. Exploration of alloy 441 chemistry for solid oxide fuel cell interconnect application. J Power Sources 2010;195:813–20. https://doi.org/10.1016/j.jpowsour.2009.08.023.
[41] Sello MP, Stumpf WE. Laves phase embrittlement of the ferritic stainless steel type AISI 441. Mater Sci Eng A 2010;527:5194–202. https://doi.org/10.1016/j.msea.2010.04.058.
[42] Barbé L, Bultinck I, Duprez L, Cooman BCD. Influence of composition on crack sensitivity of ferritic stainless steel. Mater Sci Technol 2002;18:664–72. https://doi.org/10.1179/026708302225003613.

[43] Kofstad P. High Temperature Corrosion. 1988.
[44] Young DJ. High temperature oxidation and corrosion of metals. vol. 1. Elsevier; 2008.
[45] Opila EJ, Myers DL, Jacobson NS, Nielsen IMB, Johnson DF, Olminsky JK, et al. Theoretical and Experimental Investigation of the Thermochemistry of $CrO_2(OH)_2$(g). J Phys Chem A 2007;111:1971–80. https://doi.org/10.1021/jp0647380.
[46] Young DJ, Zurek J, Singheiser L, Quadakkers WJ. Temperature dependence of oxide scale formation on high-Cr ferritic steels in Ar–H2–H2O. Corros Sci 2011;53:2131–41. https://doi.org/10.1016/j.corsci.2011.02.031.
[47] Talic B, Molin S, Hendriksen PV, Lein HL. Effect of pre-oxidation on the oxidation resistance of Crofer 22 APU. Corros Sci 2018. https://doi.org/10.1016/j.corsci.2018.04.016.
[48] Liu H, Stack MM, Lyon SB. Reactive element effects on the ionic transport processes in Cr2O3 scales. Solid State Ion 1998;109:247–57. https://doi.org/10.1016/S0167-2738(98)00101-5.
[49] Casteel M, Lewis D, Willson P, Alinger M. Ionic Conductivity Method for measuring vaporized chromium species from solid oxide fuel cell interconnects. Int J Hydrog Energy 2012;37:6818–29. https://doi.org/10.1016/j.ijhydene.2012.01.016.
[50] Hindam H, Whittle DP. Microstructure, adhesion and growth kinetics of protective scales on metals and alloys. Oxid Met 1982;18:245–84. https://doi.org/10.1007/BF00656571.
[51] Quadakkers WJ, Holzbrecher H, Briefs KG, Beske H. Differences in growth mechanisms of oxide scales formed on ODS and conventional wrought alloys. Oxid Met 1989;32:67–88. https://doi.org/10.1007/BF00665269.
[52] Chevalier S, Bonnet G, Fielitz P, Strehl G, Weber S, Borchardt G, et al. Effects of a Reactive Element on isothermal and cyclic oxidation of chromia-forming alloys: SEM/EDX,TEM and SIMS investigations. Mater High Temp 2000;17:247–55. https://doi.org/10.1179/mht.2000.17.2.011.
[53] Huczkowski P, Christiansen N, Shemet V, Niewolak L, Piron-Abellan J, Singheiser L, et al. Growth Mechanisms and Electrical Conductivity of Oxide Scales on Ferritic Steels Proposed as Interconnect Materials for SOFC's. Fuel Cells 2006;6:93–9. https://doi.org/10.1002/fuce.200500110.
[54] Kofstad P, Lillerud KP. On High Temperature Oxidation of Chromium II . Properties of and the Oxidation Mechanism of Chromium. J Electrochem Soc 1980;127:2410–9. https://doi.org/10.1149/1.2129481.
[55] Holt A, Kofstad P. Electrical conductivity of Cr2O3 doped with TiO2. Solid State Ion 1999;117:21–5. https://doi.org/10.1016/S0167-2738(98)00244-6.
[56] Toscan F, Antoni L, Wouters Y, Dupeux M, Galerie A. Oxidation Kinetics and Scale Spallation of Iron-Chromium Alloys with Different Titanium Contents. Mater Sci Forum 2004. https://doi.org/10.4028/www.scientific.net/MSF.461-464.705.
[57] Seo HS, Yun DW, Kim KY. Effect of Ti addition on the electric and ionic property of the oxide scale formed on the ferritic stainless steel for SOFC interconnect. Int J Hydrog Energy 2012;37:16151–60. https://doi.org/10.1016/j.ijhydene.2012.08.073.
[58] Seo HS, Yun DW, Kim KY. Oxidation behavior of ferritic stainless steel containing Nb, Nb–Si and Nb–Ti for SOFC interconnect. Int J Hydrog Energy 2013;38:2432–42. https://doi.org/10.1016/j.ijhydene.2012.12.073.
[59] Niewolak L, Savenko A, Grüner D, Hattendorf H, Breuer U, Quadakkers WJ. Temperature Dependence of Laves Phase Composition in Nb, W and Si-Alloyed High Chromium Ferritic Steels

for SOFC Interconnect Applications. J Phase Equilibria Diffus 2015;36:471–84. https://doi.org/10.1007/s11669-015-0403-5.
[60] Linder M, Hocker T, Holzer L, Friedrich KA, Iwanschitz B, Mai A, et al. Model-based prediction of the ohmic resistance of metallic interconnects from oxide scale growth based on scanning electron microscopy. J Power Sources 2014;272:595–605. https://doi.org/10.1016/j.jpowsour.2014.08.098.
[61] Liu W, Sun X, Stephens E, Khaleel M. Interfacial Shear Strength of Oxide Scale and SS 441 Substrate. Metall Mater Trans A 2011;42:1222–8. https://doi.org/10.1007/s11661-010-0537-3.
[62] Schütze M. Mechanical properties of oxide scales. Oxid Met 1995;44:29–61. https://doi.org/10.1007/BF01046722.
[63] Belogolovsky I, Hou PY, Jacobson CP, Visco SJ. Chromia scale adhesion on 430 stainless steel: Effect of different surface treatments. J Power Sources 2008;182:259–64. https://doi.org/10.1016/j.jpowsour.2008.03.080.
[64] Chou Y-S, Stephens E, Xu Z, Xu W, Koeppel B, Stevenson J. Mitigation and Prediction of Spallation of Oxide Scales on Ferritic Stainless Steel. Pacific Northwest National Laboratory (PNNL), Richland, WA (US); 2015.
[65] Gambino LV, Magdefrau NJ, Aindow M. Microstructural effects of the reduction step in reactive consolidation of manganese cobaltite coatings on Crofer 22 APU. Mater High Temp 2015;32:142–7. https://doi.org/10.1179/0960340914Z.00000000090.
[66] Lee S-I, Hong J, Kim H, Son J-W, Lee J-H, Kim B-K, et al. Highly Dense Mn-Co Spinel Coating for Protection of Metallic Interconnect of Solid Oxide Fuel Cells. J Electrochem Soc 2014;161:F1389–94. https://doi.org/10.1149/2.0541414jes.
[67] Kidner NJ, Nextech Coatings. Protective Coatings for Metallic SOFC Components 2012.
[68] Akanda SR, Kidner NJ, Walter ME. Spinel coatings on metallic interconnects: Effect of reduction heat treatment on performance. Surf Coat Technol 2014;253:255–60. https://doi.org/10.1016/j.surfcoat.2014.05.049.
[69] Horita T, Kishimoto H, Yamaji K, Xiong Y, Brito ME, Yokokawa H, et al. Diffusion of oxygen in the scales of Fe–Cr alloy interconnects and oxide coating layer for solid oxide fuel cells. Solid State Ion 2008;179:2216–21. https://doi.org/10.1016/j.ssi.2008.07.024.
[70] Kurokawa H, Jacobson CP, DeJonghe LC, Visco SJ. Chromium vaporization of bare and of coated iron–chromium alloys at 1073 K. Solid State Ion 2007;178:287–96. https://doi.org/10.1016/j.ssi.2006.12.010.
[71] Trebbels R, Markus T, Singheiser L. Investigation of Chromium Vaporization from Interconnector Steels with Spinel Coatings. J Electrochem Soc 2010;157:B490–5. https://doi.org/10.1149/1.3298434.
[72] Fontana S, Chevalier S, Caboche G. Metallic Interconnects for Solid Oxide Fuel Cell: Performance of Reactive Element Oxide Coating During 10, 20 and 30 Months Exposure. Oxid Met 2012;78:307–28. https://doi.org/10.1007/s11085-012-9308-4.
[73] Stott FH, Wood GC, Stringer J. The influence of alloying elements on the development and maintenance of protective scales. Oxid Met 1995;44:113–45. https://doi.org/10.1007/BF01046725.